CONFIDENTIAL

X63 15206

CODE-2

34 p.

NASA

TECHNICAL MEMORANDUM

X-844

PRELIMINARY AERODYNAMIC CHARACTERISTICS OF A

MANNED LIFTING ENTRY VEHICLE AT A

MACH NUMBER OF 6.8

By Robert W. Rainey and Charles L. Ladson

Langley Research Center
Langley Station, Hampton, Va.

NATIONAL AERONAUTICS AND SPACE ADMINISTRATION

WASHINGTON

August 1963

CONFIDENTIAL

NOFORN

ERRATA

NASA Technical Memorandum X-844

PRELIMINARY AERODYNAMIC CHARACTERISTICS OF A
MANNED LIFTING ENTRY VEHICLE AT A
MACH NUMBER OF 6.8

By Robert W. Rainey and Charles L. Ladson
August 1963

Page 32: An error has been noted in the key of figure 7. The key should be
corrected to read as follows:

      ◯ HL-10 (tails off)
      □ HL-10
      ◇ HL-11 (tails off)
      △ HL-11

Issued 2-14-64

TECHNICAL MEMORANDUM X-844

PRELIMINARY AERODYNAMIC CHARACTERISTICS OF A

MANNED LIFTING ENTRY VEHICLE AT A

MACH NUMBER OF 6.8*

By Robert W. Rainey and Charles L. Ladson

SUMMARY

At the Langley Research Center a study is underway of the aerodynamic characteristics from subsonic to hypersonic speeds of a manned lifting entry vehicle (MLEV) with a hypersonic maximum lift-drag ratio of about 1. Preliminary results at a Mach number of 6.8 of this cambered, flat-bottom, blunt-leading-edge, delta-planform configuration show that desired performance was achieved at a moderate lift coefficient with stability and trim capability over a wide range of angle of attack and lift. Significant differences in trim attitude and directional stability occurred as a result of change in configuration camber.

INTRODUCTION

An extensive review of the manned entry study being conducted at the Langley Research Center, some results of which are reported in reference 1, has indicated that an entry vehicle with a maximum hypersonic lift-drag ratio of about 1 merits further consideration from the standpoint of possible requirements for future entry vehicles. From this review and other examinations interest has evolved in a cambered, flat-bottom, blunt-leading-edge, thick, delta wing, and an investigation is underway at speeds from subsonic to hypersonic to study the aerodynamic problems associated with one or two of the more promising configurations in this class of entry vehicles.

The purpose of this report is to present some of the results of the initial hypersonic tests. These tests were conducted in the Langley 11-inch hypersonic tunnel at a Mach number of 6.8 and Reynolds numbers, based on model length, of about 1.5×10^6 and 2.0×10^6. The results are presented without extensive analysis.

b   characteristic span for yawing-moment and rolling-moment coefficients, 5.155 inches

C_A axial-force coefficient, Axial force/$q_\infty S$

C_D drag coefficient, Drag/$q_\infty S$

C_L lift coefficient, Lift/$q_\infty S$

C_l rolling-moment coefficient, Rolling moment/$q_\infty Sb$

$C_{l_\beta} = \dfrac{\partial C_l}{\partial \beta}$ per degree

C_m pitching-moment coefficient, Pitching moment/$q_\infty S l$

C_N normal-force coefficient, Normal force/$q_\infty S$

C_n yawing-moment coefficient, Yawing moment/$q_\infty Sb$

$C_{n_\beta} = \dfrac{\partial C_n}{\partial \beta}$ per degree

C_Y side-force coefficient, Side force/$q_\infty S$

$C_{Y_\beta} = \dfrac{\partial C_Y}{\partial \beta}$ per degree

L/D   lift-drag ratio

l length of vehicle, 8.00 inches

M_∞ free-stream Mach number

q_∞ free-stream dynamic pressure

S   reference area equal to projected planform area with elevons

S_e elevon area

X,Y,Z   body axes (see fig. 1)

y,z   ordinates along body axes

2

α angle of attack, deg

β angle of sideslip, deg

δ_e elevon deflection angle, positive with trailing edge down, deg; used with subscripts L and R to indicate left elevon deflection and right elevon deflection, respectively

CONFIGURATION CONCEPTS

The results reported herein represent only the initial phase of a much broader overall study directed toward demonstrating satisfactory aerodynamic characteristics for the class of vehicle advanced in reference 1. In arriving at a basic configuration for this vehicle class, the criteria to be met were

(1) high lift capability at hypersonic speeds

(2) hypersonic maximum $L/D \approx 1$ at moderate to high lift

(3) satisfactory aerodynamic characteristics for operation from hypersonic to subsonic speeds (including conventional landing)

(4) volume distribution amenable to layout of internal systems with a reasonable center-of-gravity location

(5) feasible shape from structural and heat protection considerations

Experience (for example, refs. 2 and 3) has indicated that high values of lift at trim with stability may be obtained by using cambered delta plates. The values of angle of attack and C_L at trim and, to a less extent, the value of maximum L/D may be adjusted by the variation of the longitudinal local slope distribution. Consequently, two models with the same area distribution but with different local slopes (HL-10 and HL-11) were tested at hypersonic speeds to evaluate the effects of camber. This effort was undertaken not only to obtain the aforementioned high value of maximum trimmed C_L but also to obtain a moderately high value of trimmed C_L without elevon deflection. Therefore, in the event of loss of elevon control, the likelihood of survival during entry is improved. The elevons have been sized to obtain near-maximum values of trimmed C_L for normal entry with negative δ_e and a maximum value of L/D of approximately 1 with positive δ_e.

The cambered flat bottom is faired into generously rounded leading edges (see section drawings in fig. 2) that have high sweep angles to reduce convective heating rates. The relatively small nose radius would hopefully strike a reasonable compromise between radiative and convective heating on and in the vicinity of the nose at high entry velocities. (See ref. 1.) The upper part of the vehicle was contoured to provide shadowing from the oncoming flow at operation attitudes for the higher speed portion of entry.

The longitudinal thickness distribution should provide a realistic volume distribution for internal stowage and placement of equipment. Maximum thickness is adequate for crew accommodation during the mission and for positioning the crew to provide visibility during landing. Although detailed internal layouts have not been made, rough estimates indicate that with uniform density throughout the usable interior the center of gravity would be located at approximately 60 percent of the vehicle length. This location compares to the centroid of internal volume at 55 percent of the length (after making a reasonable allowance for structure beneath the outer surface). Therefore, it is felt that by appropriate location of internal equipment the center-of-gravity location at about 53 percent of the vehicle length (based on aerodynamic considerations) is reasonable. The shape also includes a hemicylinder faired into the upper surface to provide attachment to the booster or service module dependent upon type and duration of the particular mission. An attempt has been made to minimize the protuberances which might complicate the structural design and heat protection approach.

MODELS, APPARATUS, AND TESTS

The general class of vehicles under consideration has been designated MLEV (manned lifting entry vehicle). Two models of a horizontal landing version (HL) of the MLEV were tested in this investigation. These models were designated HL-10 and HL-11 and differed mainly in the camber of the lower surface. Drawings and photographs of the models are presented in figures 2 and 3, respectively. The models were constructed of stainless steel and were equipped with interchangeable elevons, fins, and rudders. Measured ordinates of the cross sections of the HL-10 and HL-11 models are presented in tables I and II, respectively.

The forces and moments were measured with a six-component strain-gage balance equipped with internal water cooling to reduce zero shifts as a result of temperature gradients. The balance entered the base of the model within the cylindrical fairing. The balance sting, behind the model trailing edge, was shrouded by a cylindrical shield 0.60 inch in diameter (fig. 4). The pressure within this shield was recorded during each test. This base pressure contribution to axial force was compared with the measured axial force and found to be negligible. Thus, the data presented are uncorrected.

A prism was mounted in the side of the model so that a light beam from a point source reflected off the prism onto a calibrated scale. In this manner, the true attitude of the model was determined irrespective of balance and support-system deflections.

The tests were conducted in the Mach 6.8 test section of the Langley 11-inch hypersonic tunnel over an angle-of-attack range from 0° to 40°. At angles of attack from 0° to 30° the tests were conducted at an average stagnation pressure of about 20 atmospheres absolute. In the Mach 6.8 test section, the average Mach number at this stagnation pressure was about 6.87. At angles of attack from 30° to 40° the tests were conducted at a stagnation pressure of about 15 atmospheres absolute at an average Mach number of about 6.82. All tests were conducted at a stagnation temperature of about 600° F. The Reynolds numbers at stagnation

pressures of 15 and 20 atmospheres were 1.5×10^6 and 2.0×10^6, respectively, based on model length.

At high angles of attack, the shock wave from the model forced separation of the boundary layer from the floor of the tunnel. The shock wave formed as a result of this separation extended into the core of good flow just downstream from the trailing edge of the model. (See fig. 4, $\alpha = 40^\circ$.) Results of tests using the same model and balance in a larger tunnel void of any such shock waves confirm that the Mach 6.8 results are free of interference at all test values of α.

ACCURACY OF RESULTS

The accuracy in angles of attack and sideslip was $\pm 0.1^\circ$. A summary of the average values and accuracies in Mach number and dynamic pressure and of the balance accuracy in terms of the aerodynamic coefficients is presented in the following table:

α, deg	M_∞	q_∞, lb/sq ft abs	Accuracy of static balance calibration in terms of -					
			C_N	C_A	C_m	C_l	C_n	C_Y
0 to 30	6.87 ± 0.03	376 ± 1.3	0.0026	0.0012	0.00032	0.000070	0.00015	0.00080
30 to 40	6.82 ± 0.03	294 ± 1.3	.0034	.0016	.00043	.000094	.00020	.0011

Mach number varied about ± 0.03 and dynamic pressure varied about 6 lb/sq ft during each test as a result of a change in tunnel throat size due to heating as each test progressed. These variations were accounted for in the data reduction.

RESULTS AND DISCUSSION

The data obtained from tests of models HL-10 and HL-11 are presented in figures 5 to 8.

The effects of camber upon the longitudinal aerodynamic characteristics of the vehicles can be seen from a comparison of figures 5(b) and 6(a). As a result of HL-11 having larger local angles of attack behind the maximum thickness where the majority of the lifting area is located, higher values of C_L and L/D were obtained for HL-11 than for HL-10. However, this higher loading on HL-11 limited the trimmed angle of attack for $\delta_e = 0^\circ$ to about 35° and a trimmed C_L to 0.37 (fig. 6(a)) as compared with $\alpha \approx 52^\circ$ and $C_L \approx 0.54$ for HL-10. These values for HL-10 at $\alpha > 40^\circ$ are obtained from extrapolation of the experimental

measurements with the aid of Newtonian theory. In addition, this higher loading on HL-11 is undoubtedly transmitted onto the sides of the rear portion of the vehicle to provide a higher level of directional stability for HL-11 than for HL-10 (fig. 7).

Although the anticipated mode of entry does not include normal operation in the low range of α at high velocities, some tests were conducted at values of α down to 0°. It is of interest to note in this low range of α the marked reduction in elevon control effectiveness of HL-10 (fig. 5(b)) as compared with the effectiveness of HL-11 (fig. 6(a)). The higher curvature and the ensuing separated flow enveloped the deflected elevons more completely for the HL-10. A solution to this problem is elevon chord-extension so that a portion of the elevon will extend beyond the separated region and penetrate the region of higher energy flow.

The hypersonic tests of the HL-11 were terminated early in the test program when the subsonic results revealed several advantages for the HL-10; consequently, the majority of the hypersonic data herein are for the HL-10. The fin and control arrangement on the HL-10 shown herein is one of several arrangements under current study.

CONCLUDING REMARKS

At the Langley Research Center a study is underway of the aerodynamic characteristics from subsonic to hypersonic speeds of a manned lifting entry vehicle with a hypersonic maximum lift-drag ratio of about 1. Preliminary results at a Mach number of 6.8 of this blunt-leading-edge delta-planform configuration show that desired performance was achieved at a moderate lift coefficient with stability and trim capability over a wide range of angle of attack and lift. Significant differences in trim attitude and directional stability occurred as a result of change in configuration camber.

Langley Research Center,
    National Aeronautics and Space Administration,
        Langley Station, Hampton, Va., May 22, 1963.

REFERENCES

1. Love, E. S., and Pritchard, E. B.: A Look at Manned Entry at Circular to Hyperbolic Velocities. Presented at the AIAA Second Manned Space Flight Symposium (Dallas, Texas), Apr. 22-24, 1963.

2. Rainey, Robert W., and Close, William H.: Studies of Stability and Control of Winged Reentry Configurations. NASA TM X-327, 1960.

3. Close, William H.: Hypersonic Longitudinal Trim, Stability, and Control Characteristics of a Delta-Wing Configuration at High Angles of Attack. NASA TM X-240, 1960.

TABLE I. HL-10 ORDINATES

Station 1		Station 2		Station 3		Station 4		Station 5		Station 6		Station 7	
y, in.	z, in.	y, in.	z, in.	y, in.	z, in.	y, in.	z, in.	y, in.	z, in.	y, in.	z, in.	y, in.	z, in.
0	0.591	0	0.647	0	0.651	0	0.651	0	0.651	0	0.651	0	0.654
.125	.569	.125	.637	.125	.647	.125	.642	.125	.634	.125	.634	.125	.636
.250	.496	.250	.607	.250	.639	.250	.627	.250	.585	.250	.564	.250	.560
.375	.349	.375	.549	.375	.617	.375	.617	.375	.569	.375	.514	.375	.440
.500	.074	.500	.454	.500	.582	.500	.601	.500	.564	.500	.502	.500	.398
.526	0	.625	.312	.625	.529	.625	.574	.625	.554	.625	.500	.625	.398
.547	-.125	.750	.074	.750	.446	.750	.541	.750	.540	.750	.497	.750	.398
.557	-.250	.781	0	.875	.318	.875	.497	.875	.522	.875	.489	.875	.398
.559	-.339	.812	-.125	1.000	.111	1.000	.432	1.000	.496	1.000	.480	1.000	.398
		.832	-.250	1.041	0	1.125	.329	1.125	.458	1.125	.469	1.125	.398
		.843	-.375	1.075	-.125	1.250	.168	1.250	.404	1.250	.454	1.250	.398
		.848	-.536	1.100	-.250	1.321	0	1.375	.331	1.375	.434	1.375	.398
				1.118	-.375	1.355	-.125	1.500	.216	1.500	.409	1.500	.398
				1.129	-.500	1.380	-.250	1.636	0	1.625	.371	1.625	.398
				1.135	-.626	1.399	-.375	1.670	-.125	1.750	.309	1.625	.398
						1.411	-.500	1.692	-.250	1.875	.209	1.875	.398
						1.415	-.620	1.704	-.375	1.984	0	2.000	.391
								1.707	-.449	1.997	-.125	2.125	.382
												2.250	.374
												2.287	0

8

TABLE II.- HL-11 ORDINATES

Station 1		Station 2		Station 3		Station 4		Station 5		Station 6		Station 7	
y, in.	z, in.	y, in.	z, in.	y, in.	z, in.	y, in.	z, in.	y, in.	z, in.	y, in.	z, in.	y, in.	z, in.
0	-0.670	0	-0.818	0	-0.867	0	-0.824	0	-0.721	0	-0.570	0	-0.386
.551	-.375	.811	-.625	1.117	-.625	1.383	-.625	1.1682	-.500	2.014	-.125	2.303	0
.563	-.250	.840	-.500	1.139	-.500	1.417	-.500	1.711	-.375	2.017	0	2.310	.125
.563	-.125	.849	-.375	1.142	-.375	1.428	-.375	1.717	-.250	2.009	.125	2.315	.250
.551	0	.851	-.250	1.139	-.250	1.430	-.250	1.716	-.125	1.976	.250	2.315	.375
.531	.125	.849	-.125	1.133	-.125	1.423	-.125	1.704	0	1.884	.375	1.500	.375
.498	.250	.840	0	1.120	0	1.407	0	1.679	.125	1.637	.500	1.000	.375
.445	.375	.823	.125	1.100	.125	1.384	.125	1.633	.250	1.375	.552	.500	.375
.358	.500	.791	.250	1.068	.250	1.341	.250	1.558	.375	1.000	.558	.375	.375
.350	.586	.744	.375	1.019	.375	1.277	.375	1.441	.500	.500	.558	.250	.466
.125	.635	.675	.500	.945	.500	1.190	.500	1.375	.548	.250	.558	.125	.542
0	.650	.625	.567	.875	.583	1.125	.568	1.250	.614	.125	.558	0	.566
0		.500	.671	.750	.688	1.000	.658	1.125	.656	0	.566		
		.375	.737	.625	.759	.875	.720	1.000	.683				
		.250	.777	.500	.803	.750	.761	.750	.708				
		.125	.796	.375	.831	.625	.789	.500	.714				
		0	.802	.250	.847	.500	.805	.250	.714				
				.125	.854	.375	.816	0	.714				
				0	.856	.250	.824						
						.125	.826						
						0	.827						
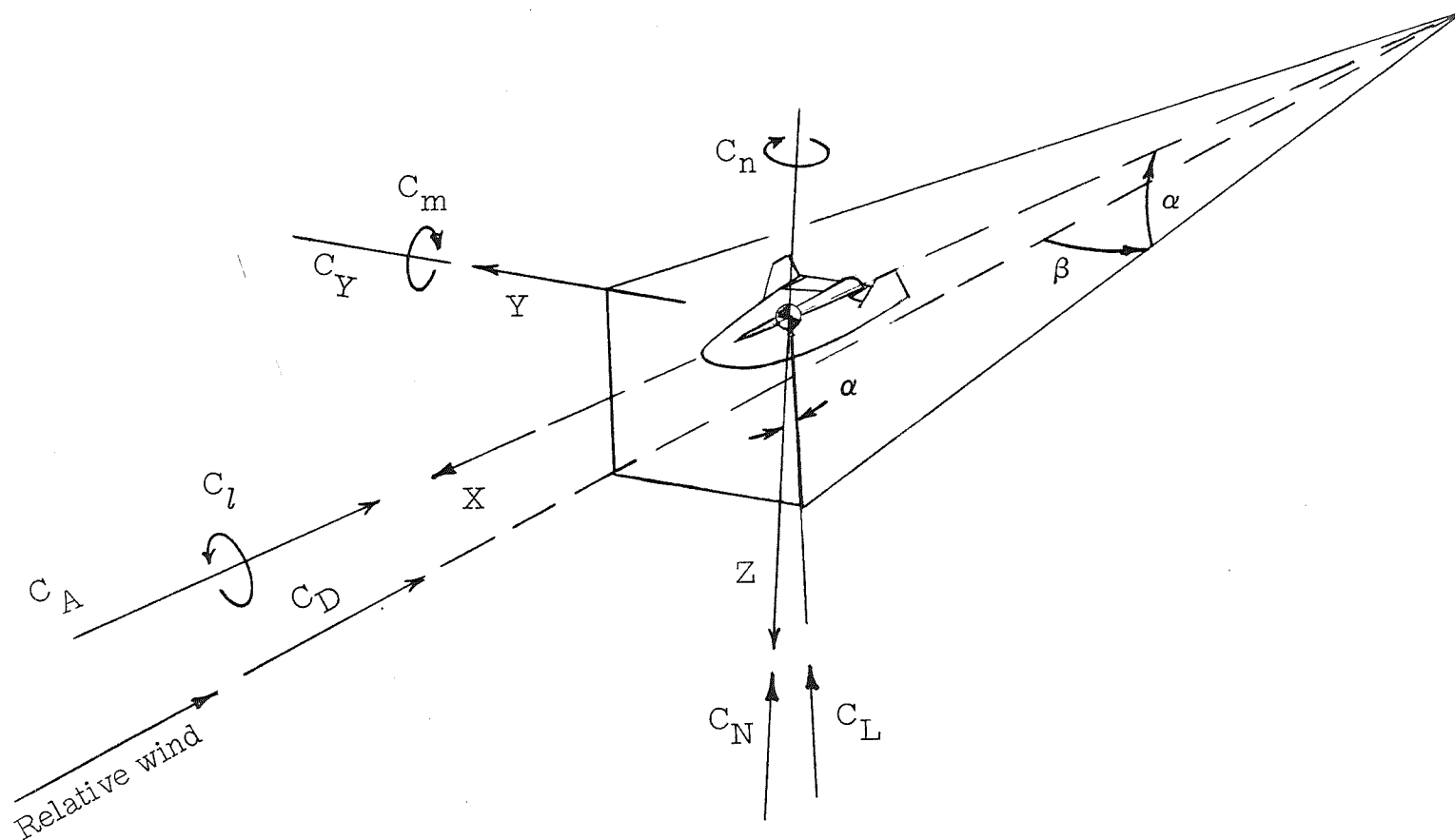
Figure 1.- Axis system with positive direction of forces, moments, and angles indicated by arrows.
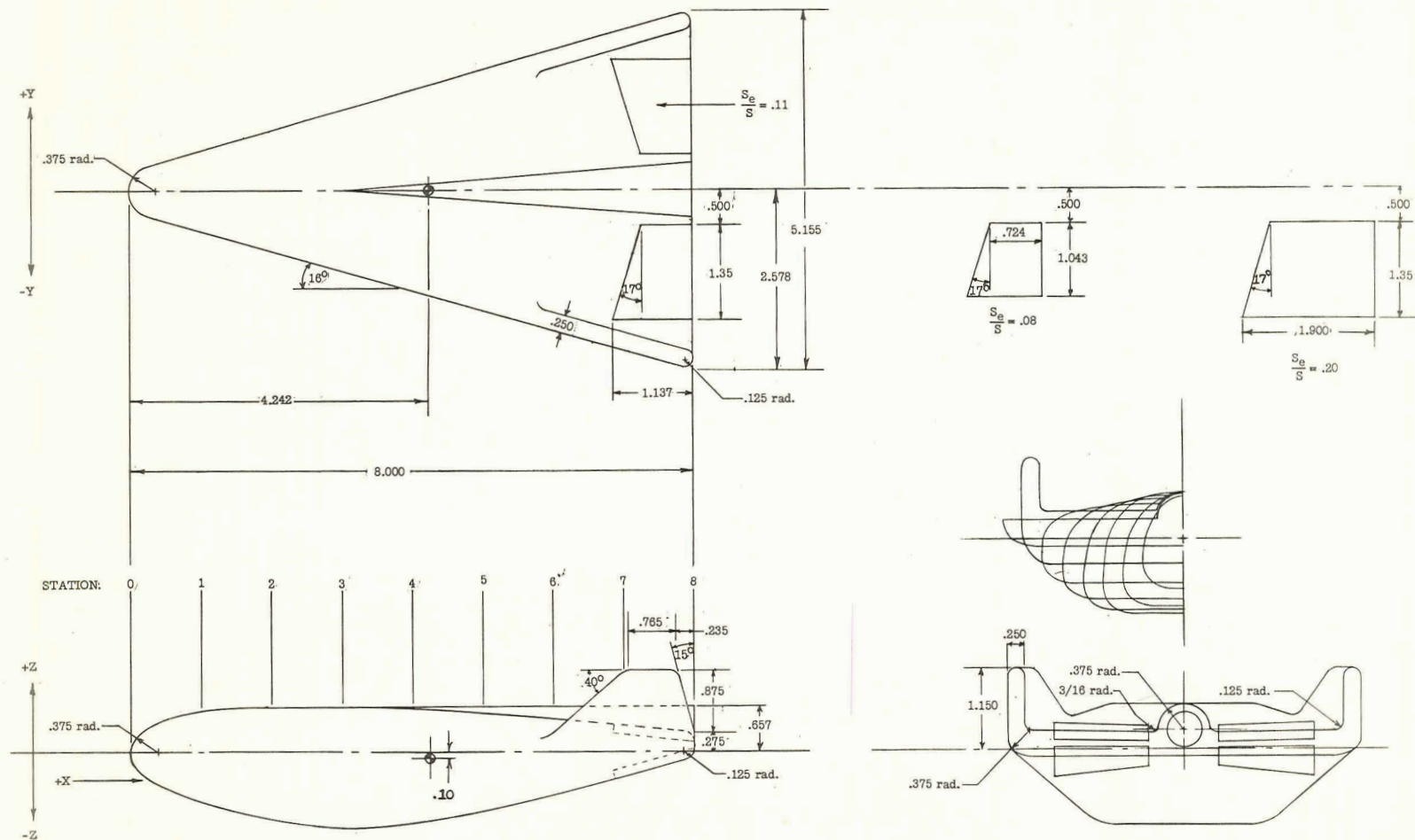
(a) HL-10 configuration.

Figure 2.- Model drawings and dimensions. All linear dimensions are in inches.
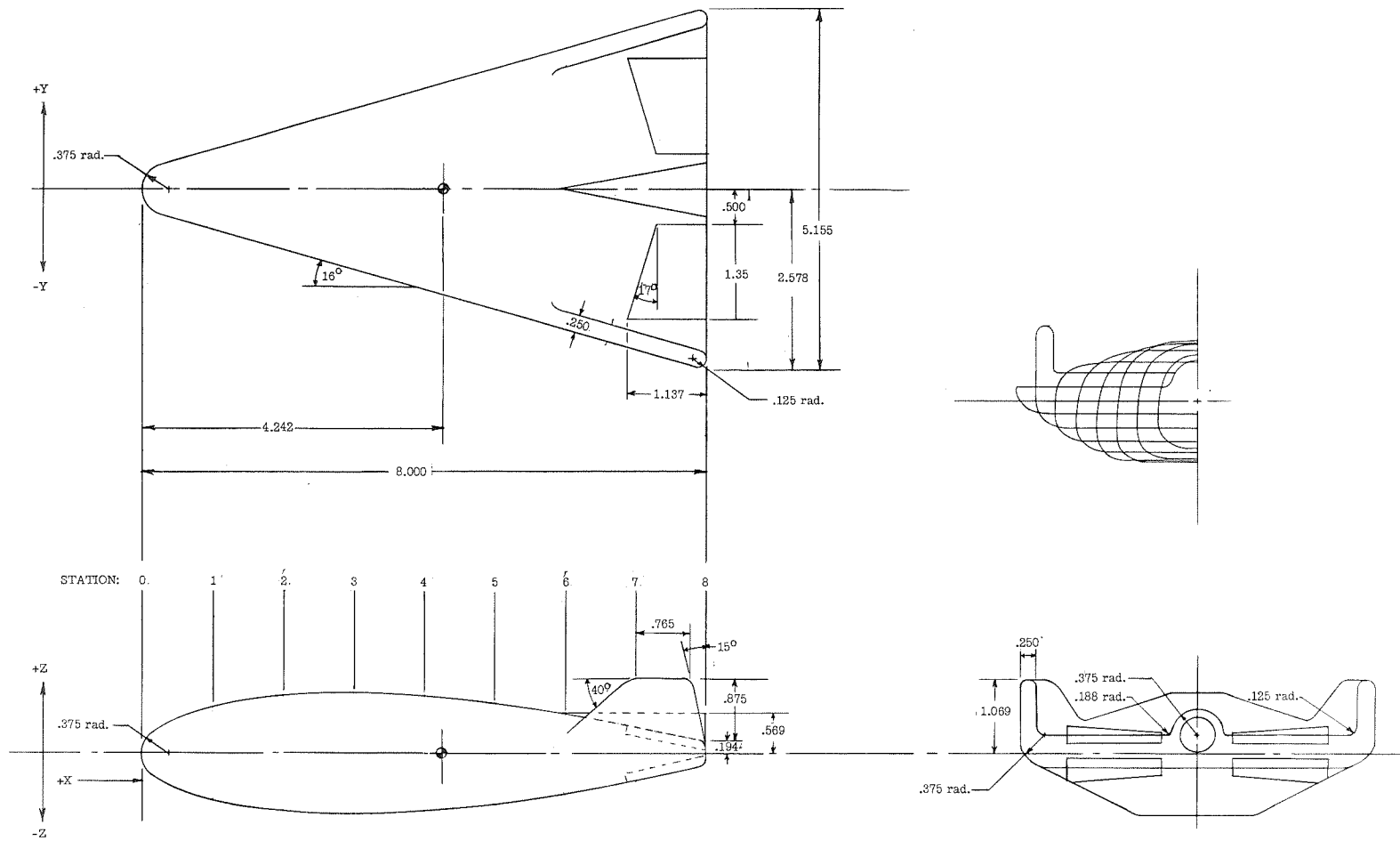
(b) HL-11 configuration.

Figure 2.- Concluded.
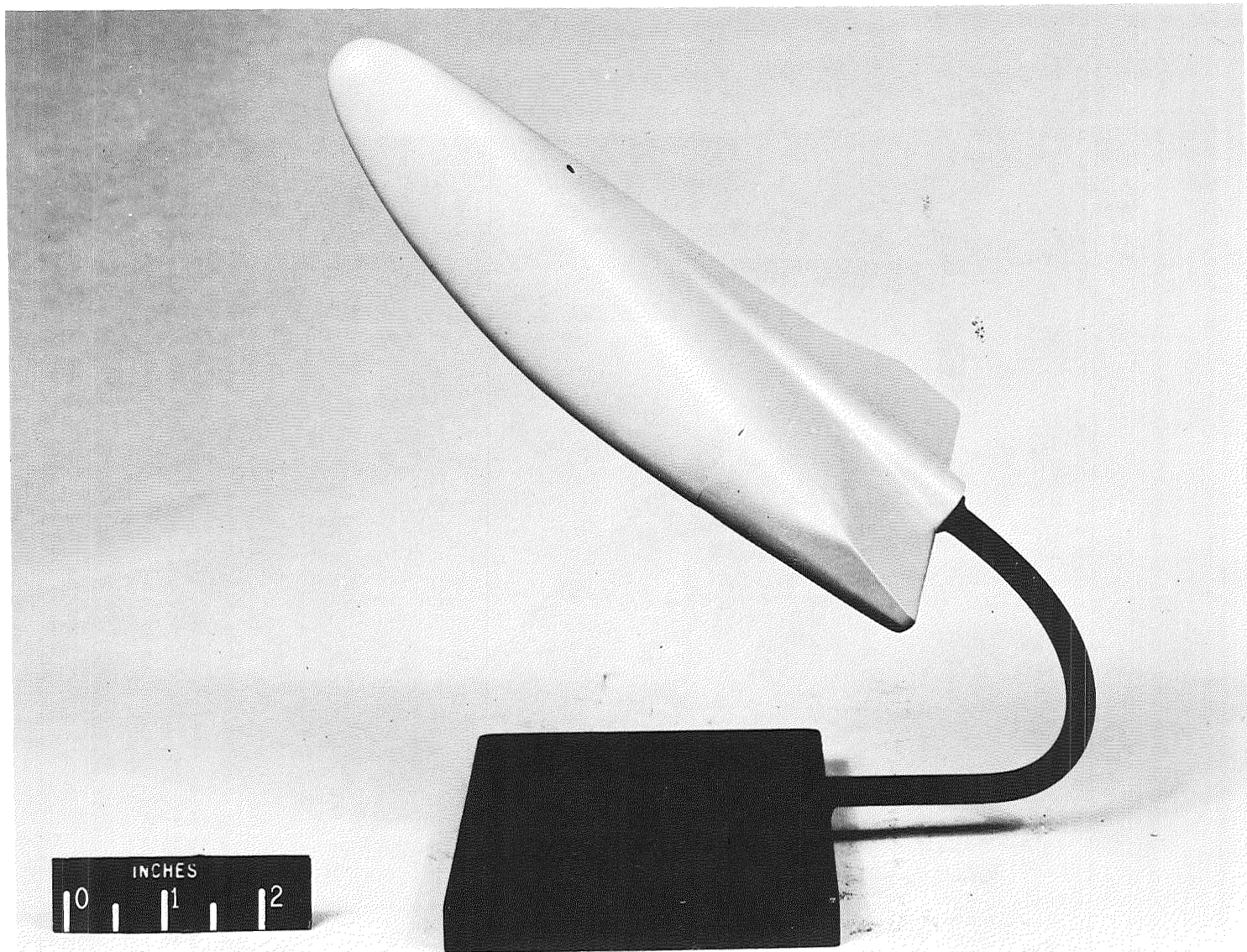
(a) HL-10; tails-off; $\delta_e = 0°$.

Figure 3.- Models used in the investigation.

L-63-2082

13
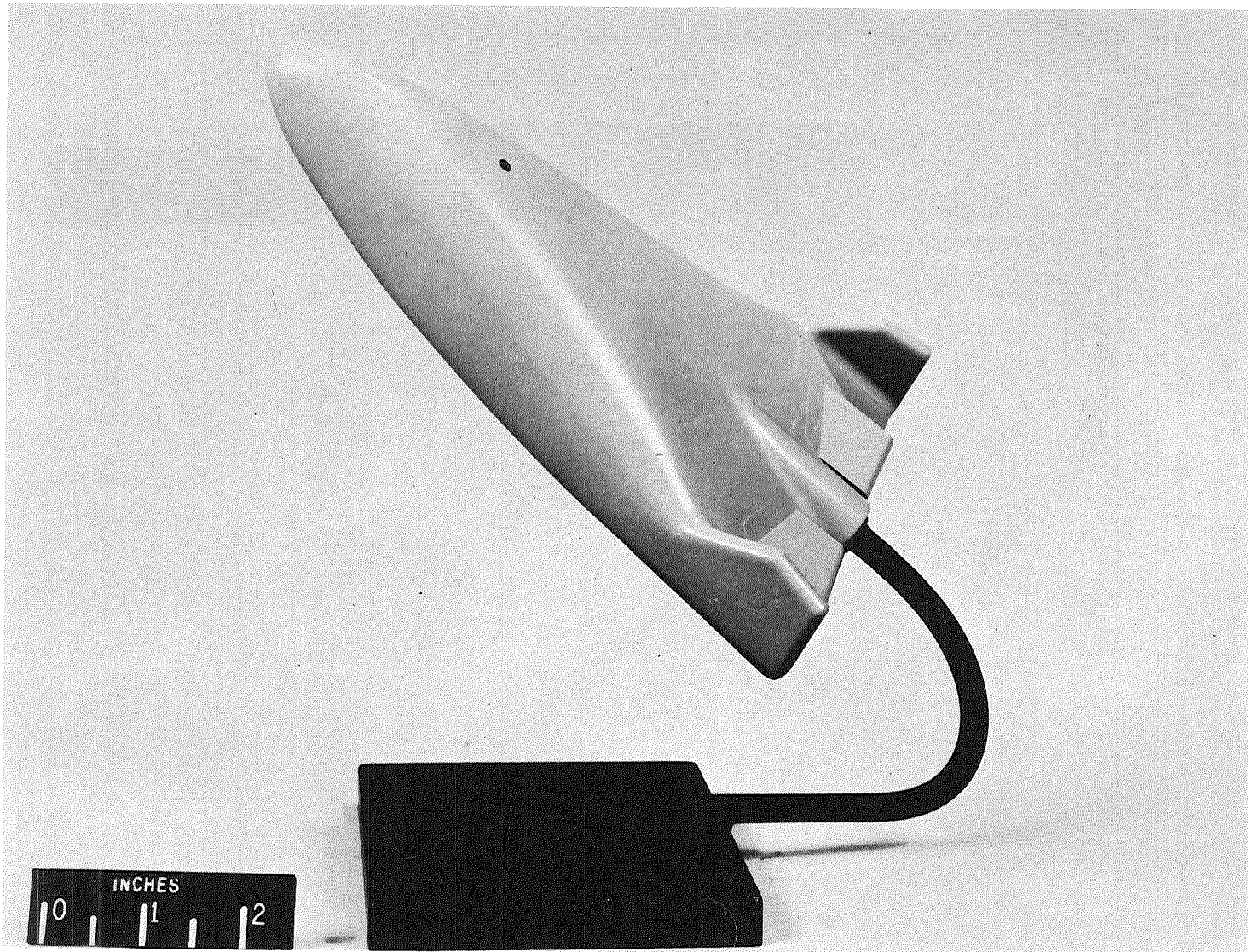
(b) HL-11; $\delta_e = -15^0$.

Figure 3.- Concluded.
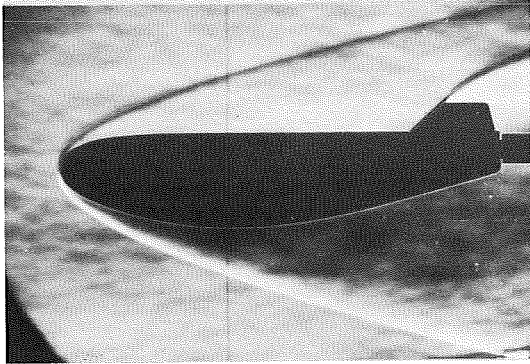
$\alpha = 0°$
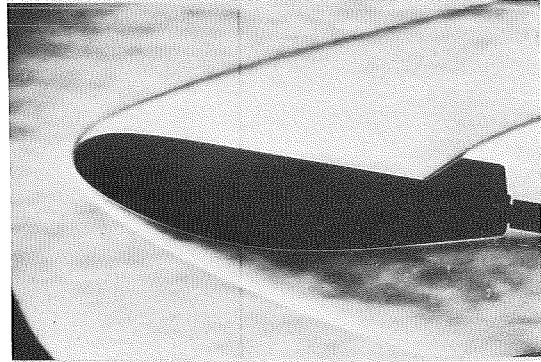
$\alpha = 10°$
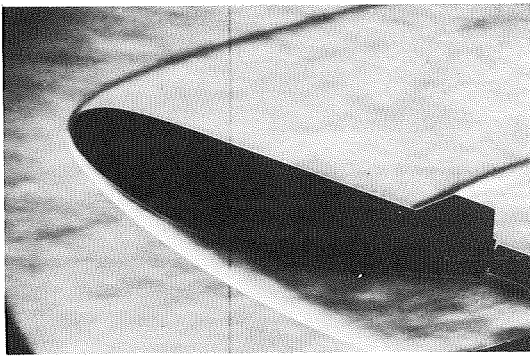
$\alpha = 20°$
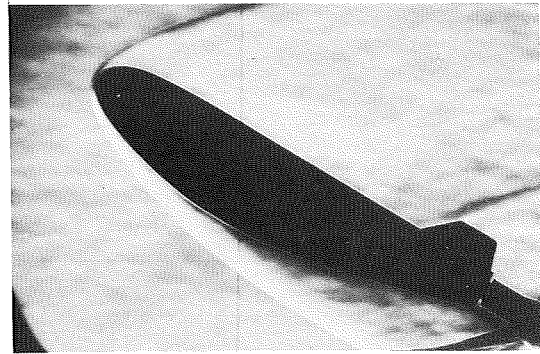
$\alpha = 30°$

(a) HL-10; $\delta_e = 0°$.

L-63-3158

Figure 4.- Schlieren flow photographs.
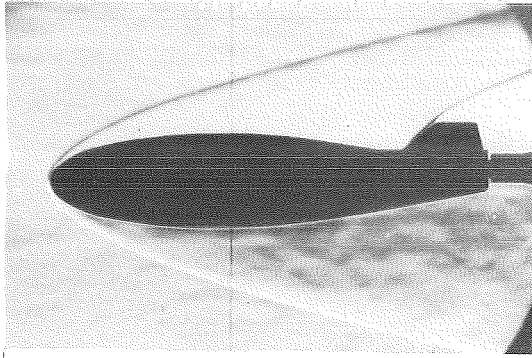
$\alpha = 0°$
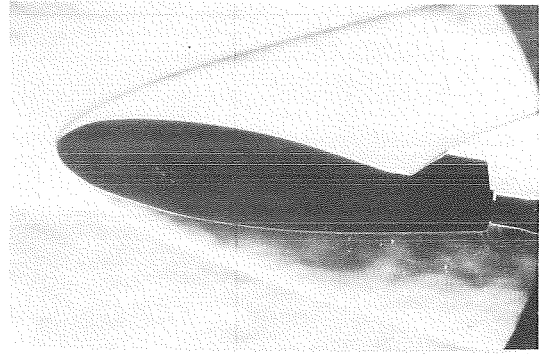
$\alpha = 10°$
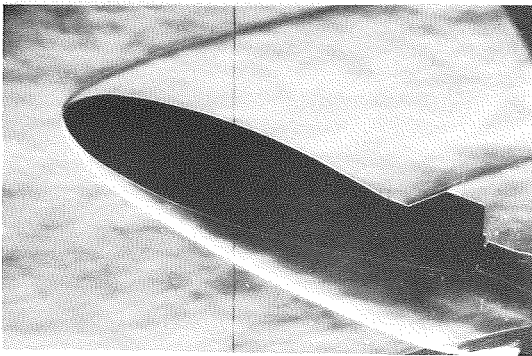
$\alpha = 20°$
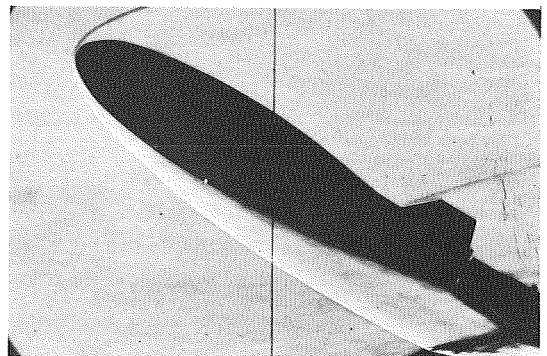
$\alpha = 30°$
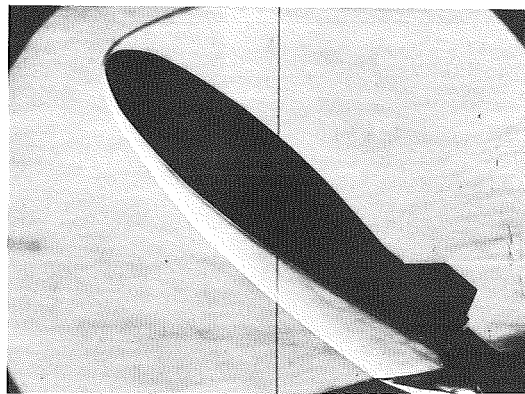
$\alpha = 40°$

(b) HL-11; $\delta_e = 0°$.

Figure 4.- Continued.

L-63-3159
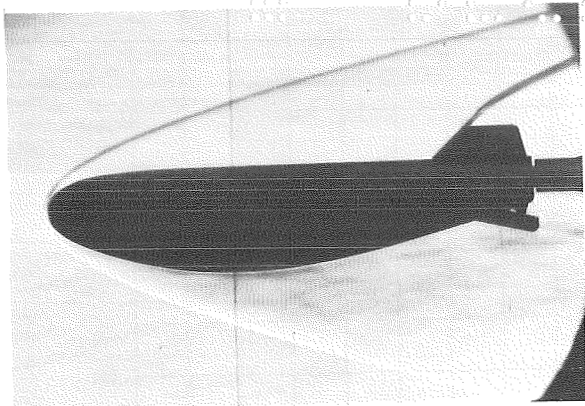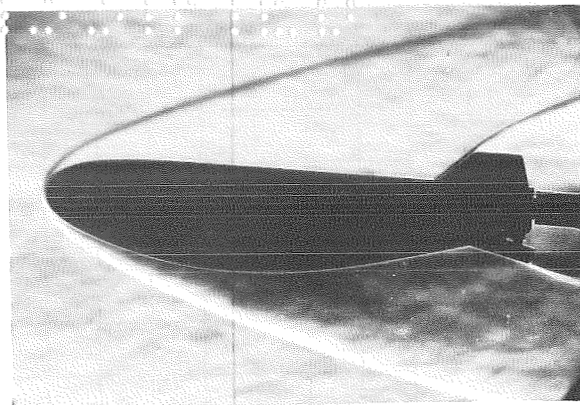
$\alpha = 0°$ $\alpha = 5°$
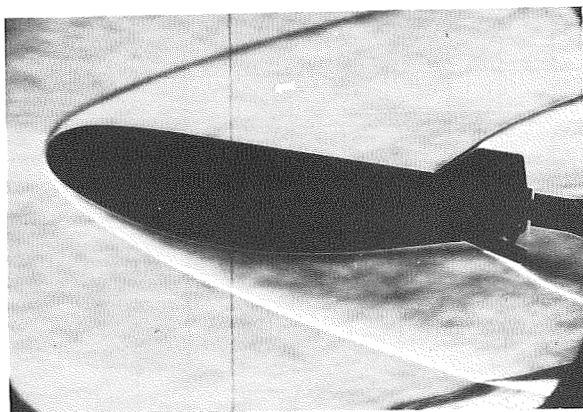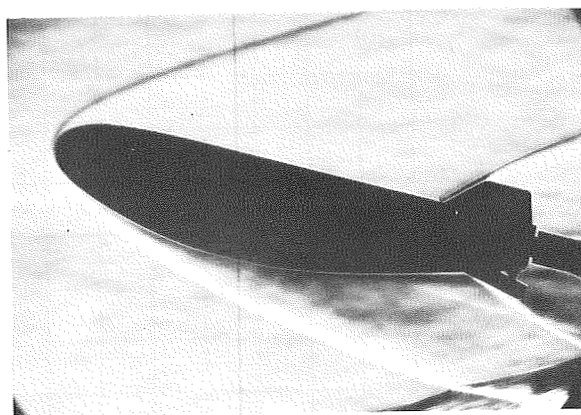
$\alpha = 10°$ $\alpha = 15°$
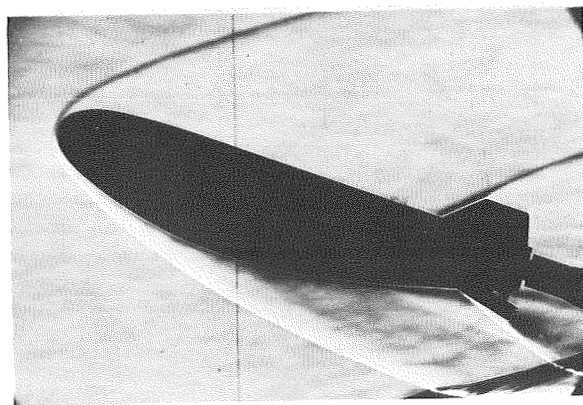
$\alpha = 20°$

(c) HL-11; $\delta_e = 30°$.   L-63-3160

Figure 4.- Concluded.
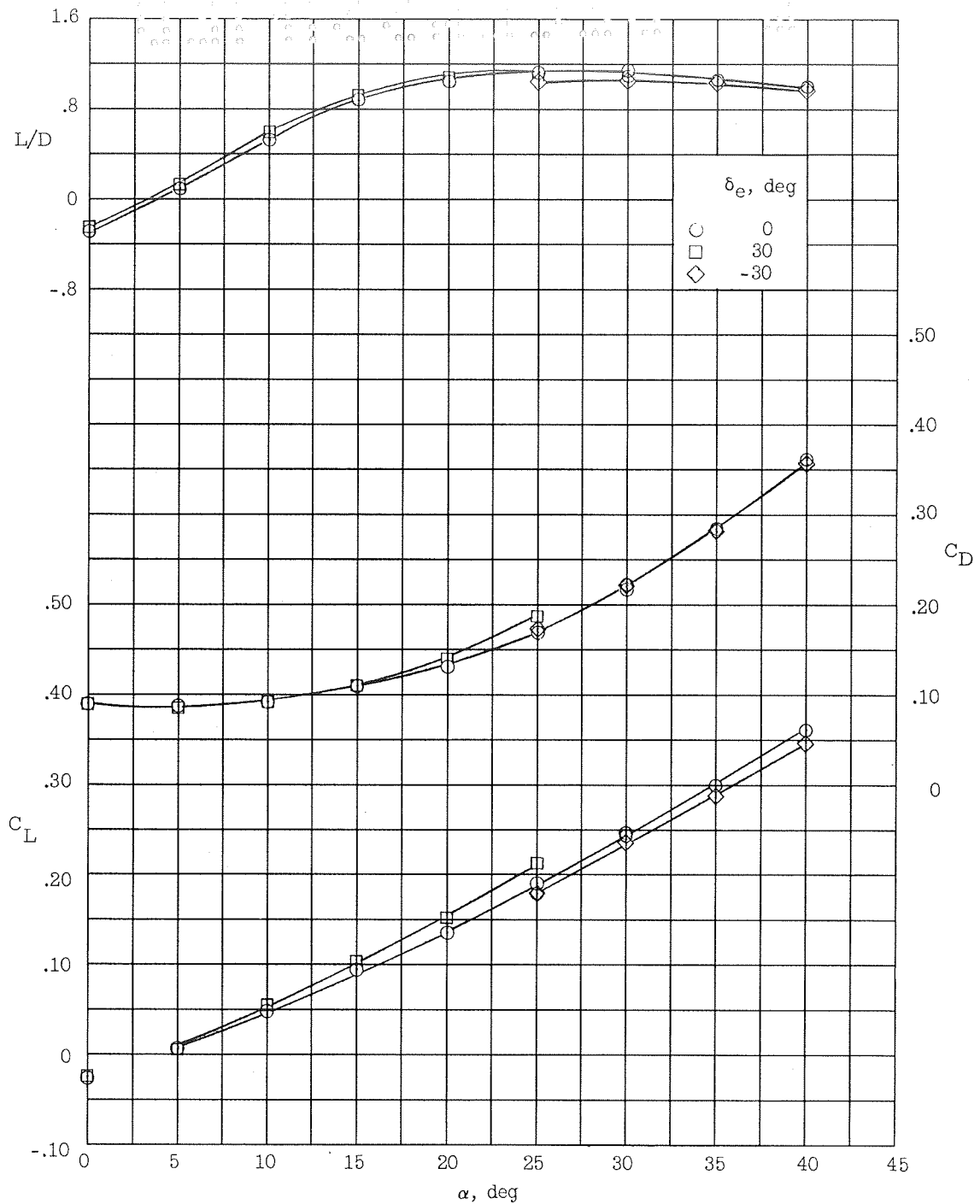
(a) Elevon-deflection effects; $\frac{S_e}{S} = 0.08$.

Figure 5.- HL-10 longitudinal aerodynamic characteristics.
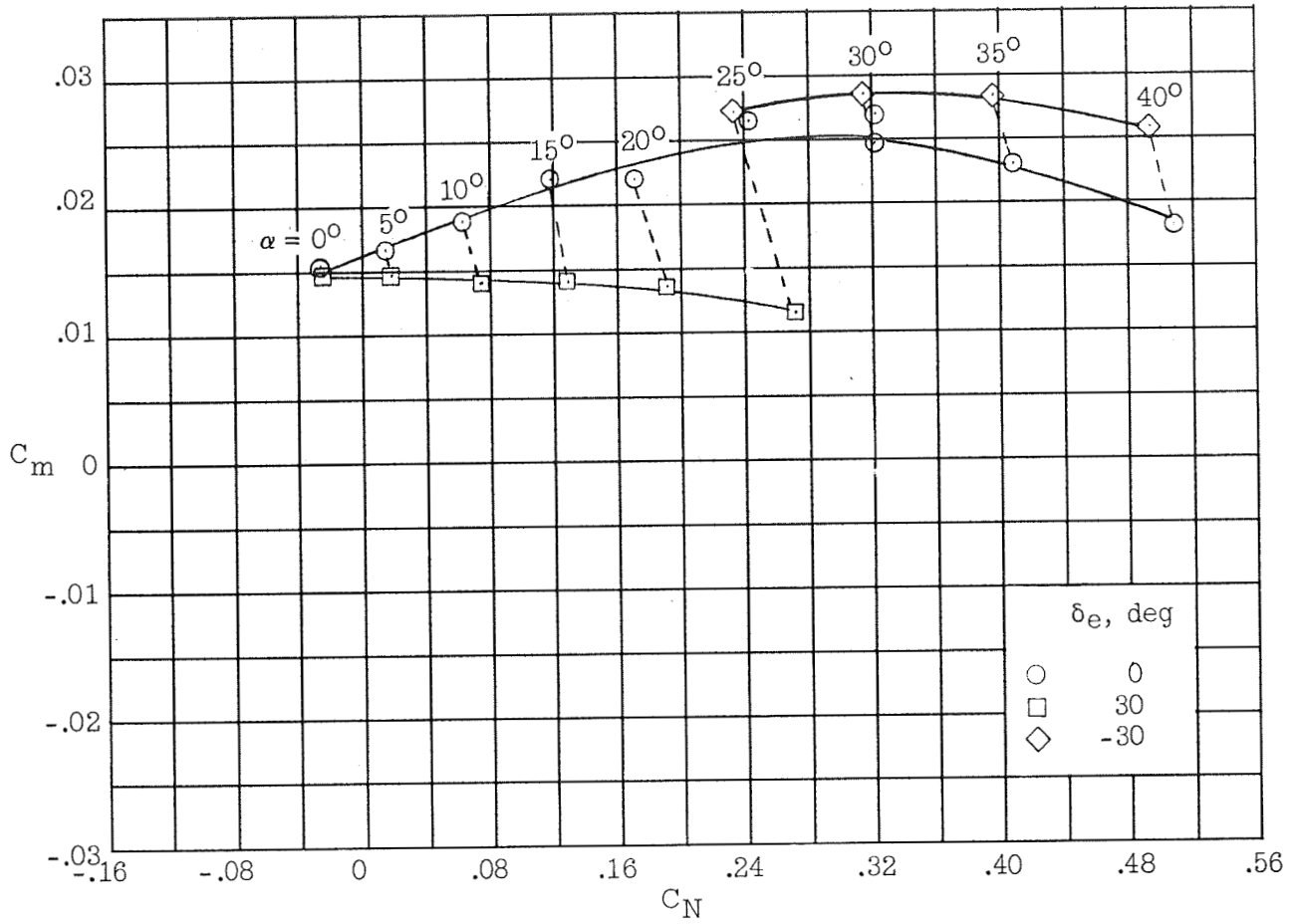
(a) Concluded.
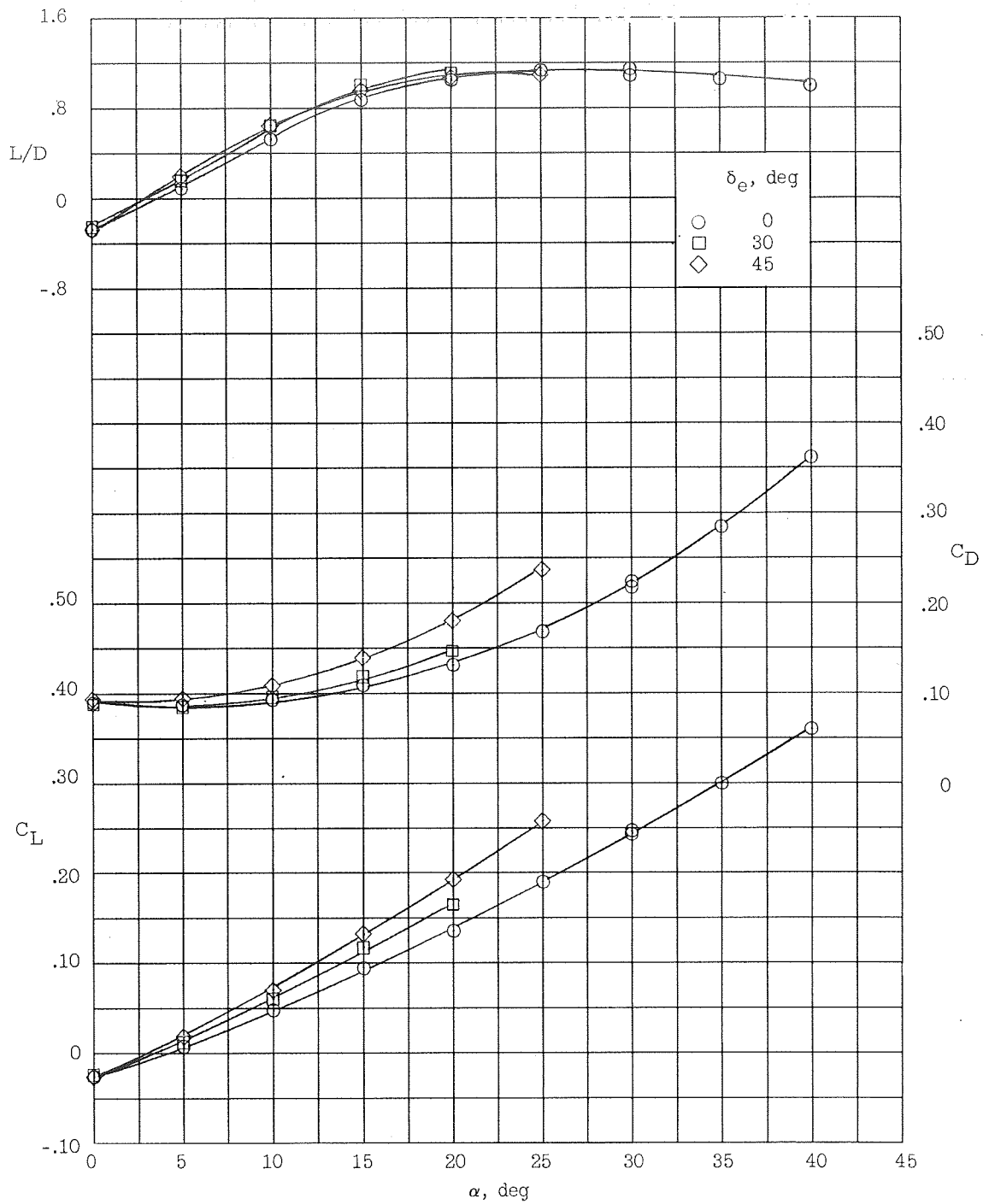
Figure 5.- Continued.

(b) Elevon-deflection effects; $\frac{S_e}{S} = 0.11$.

Figure 5.- Continued.
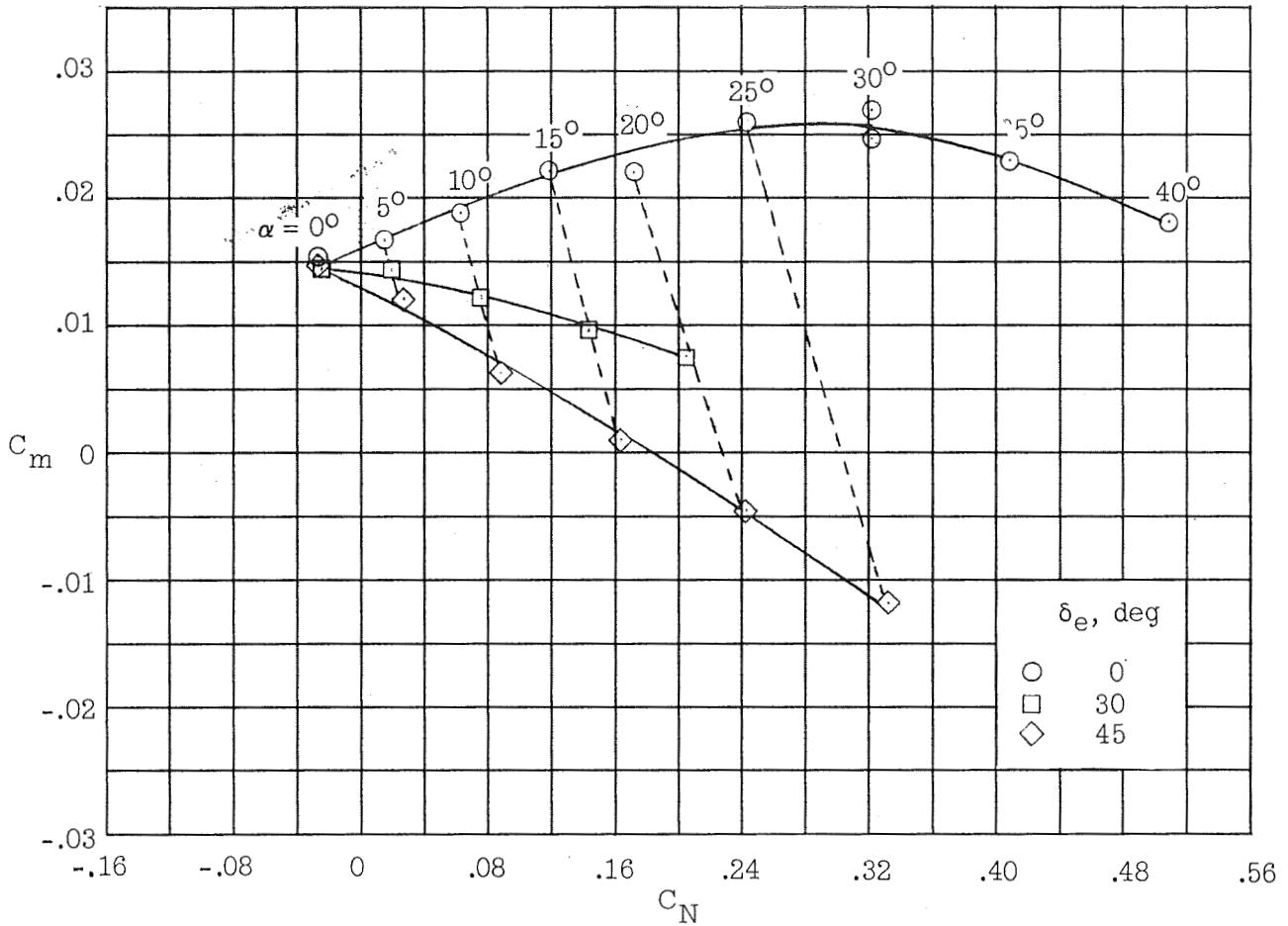
(b) Concluded.
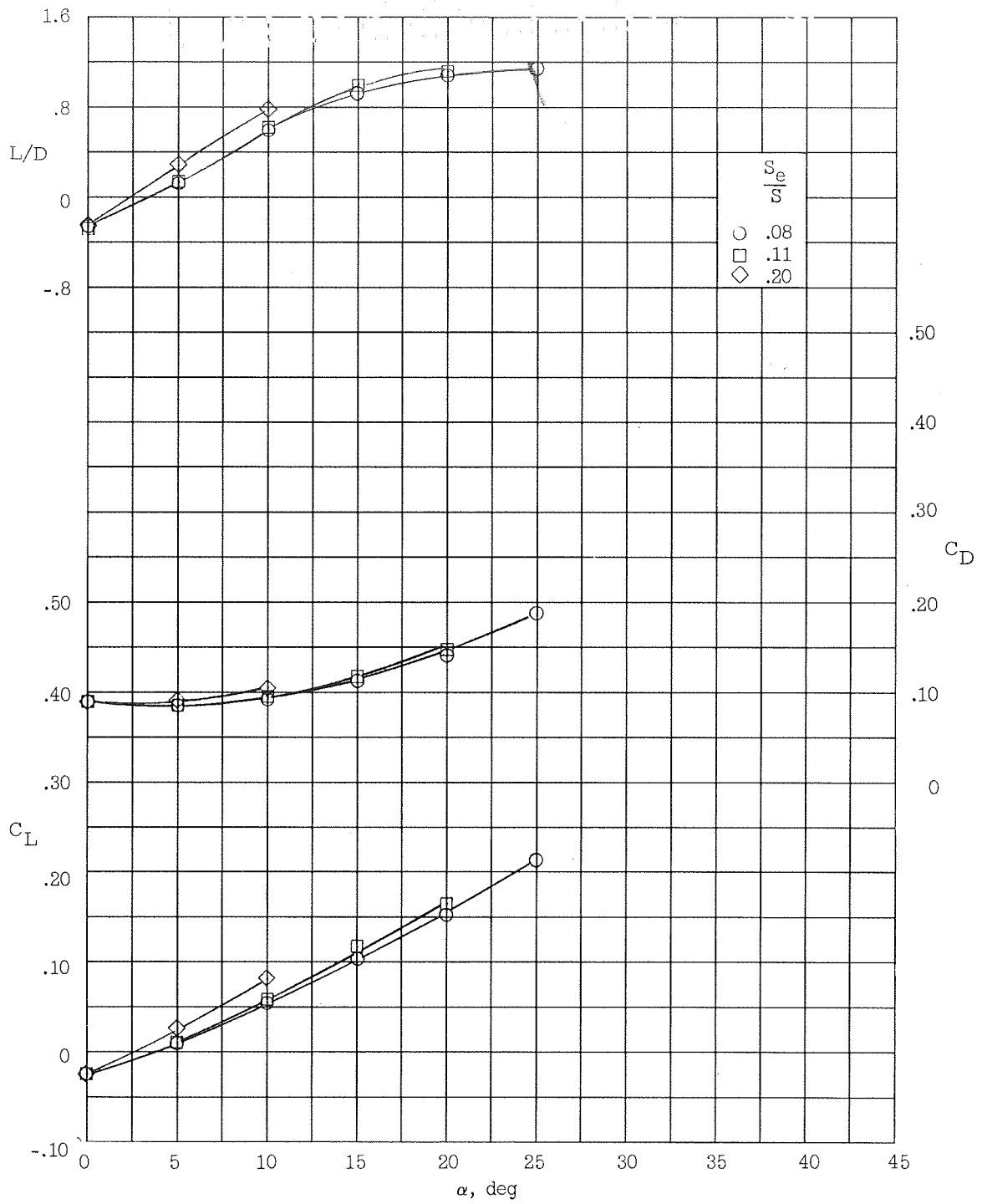
Figure 5.- Continued.

(c) Elevon-area variation; $\delta_e = 30°$.

Figure 5.- Continued.
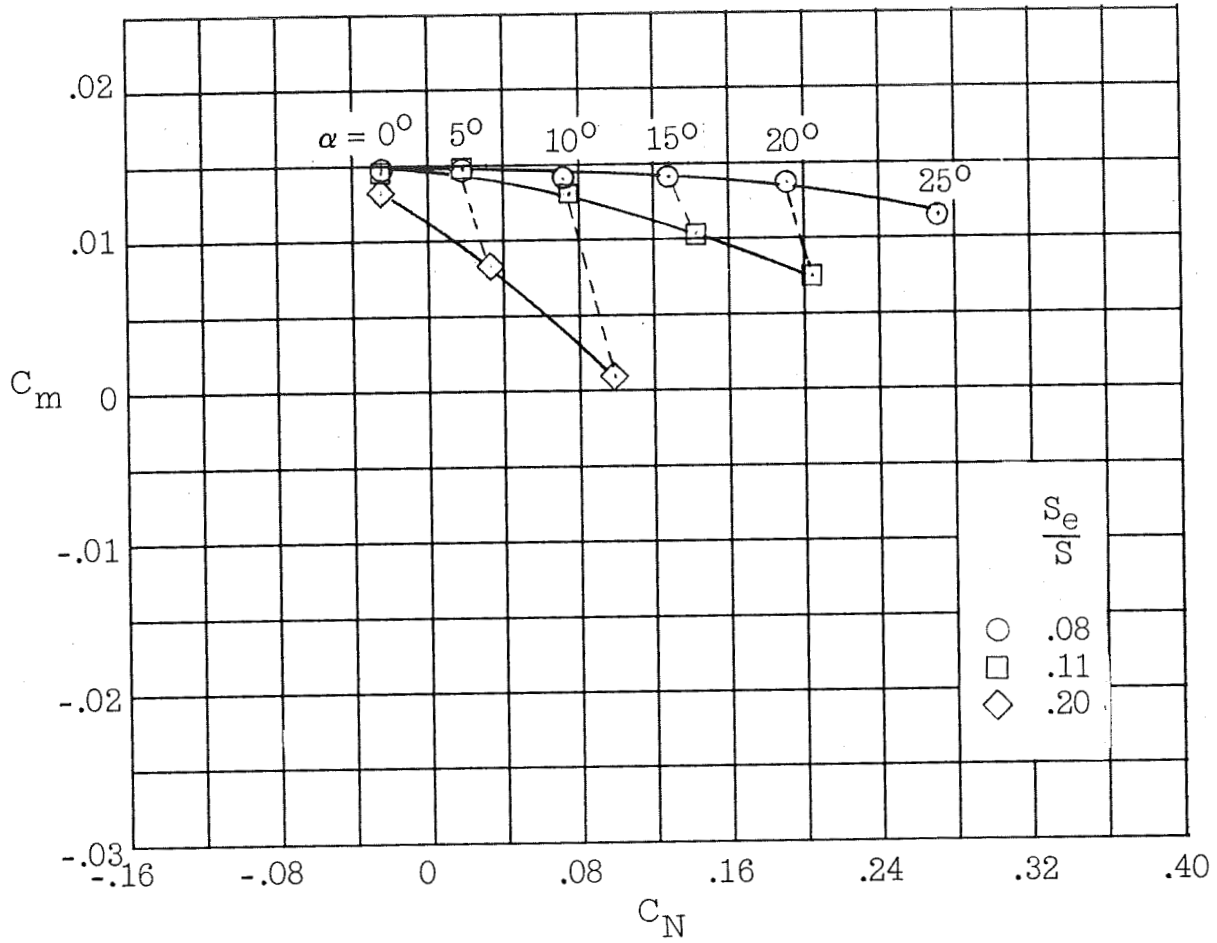
(c) Concluded.

Figure 5.- Continued.
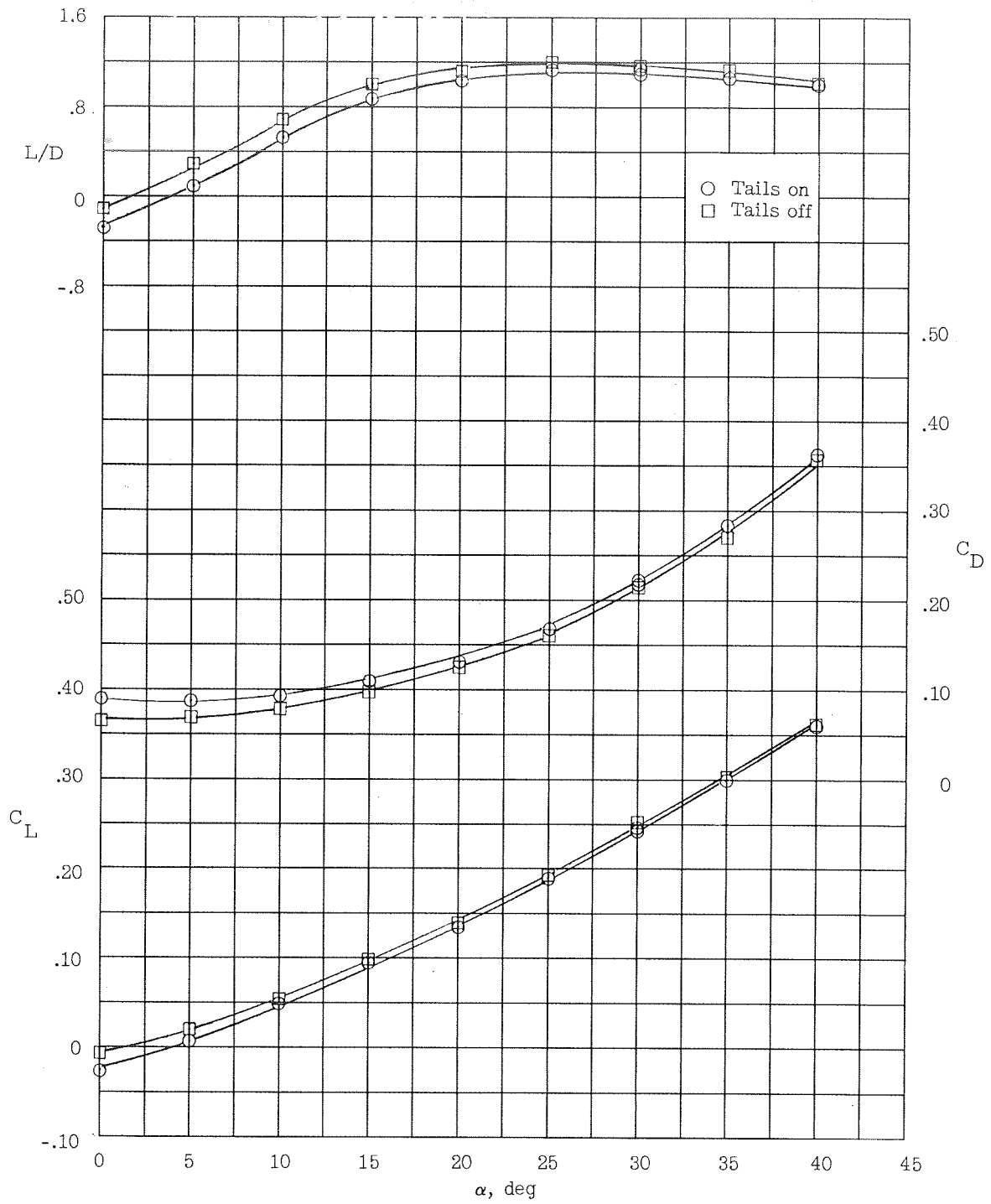
(d) Twin-dorsal-tail effects; $\delta_e = 0^\circ$.

Figure 5.- Continued.
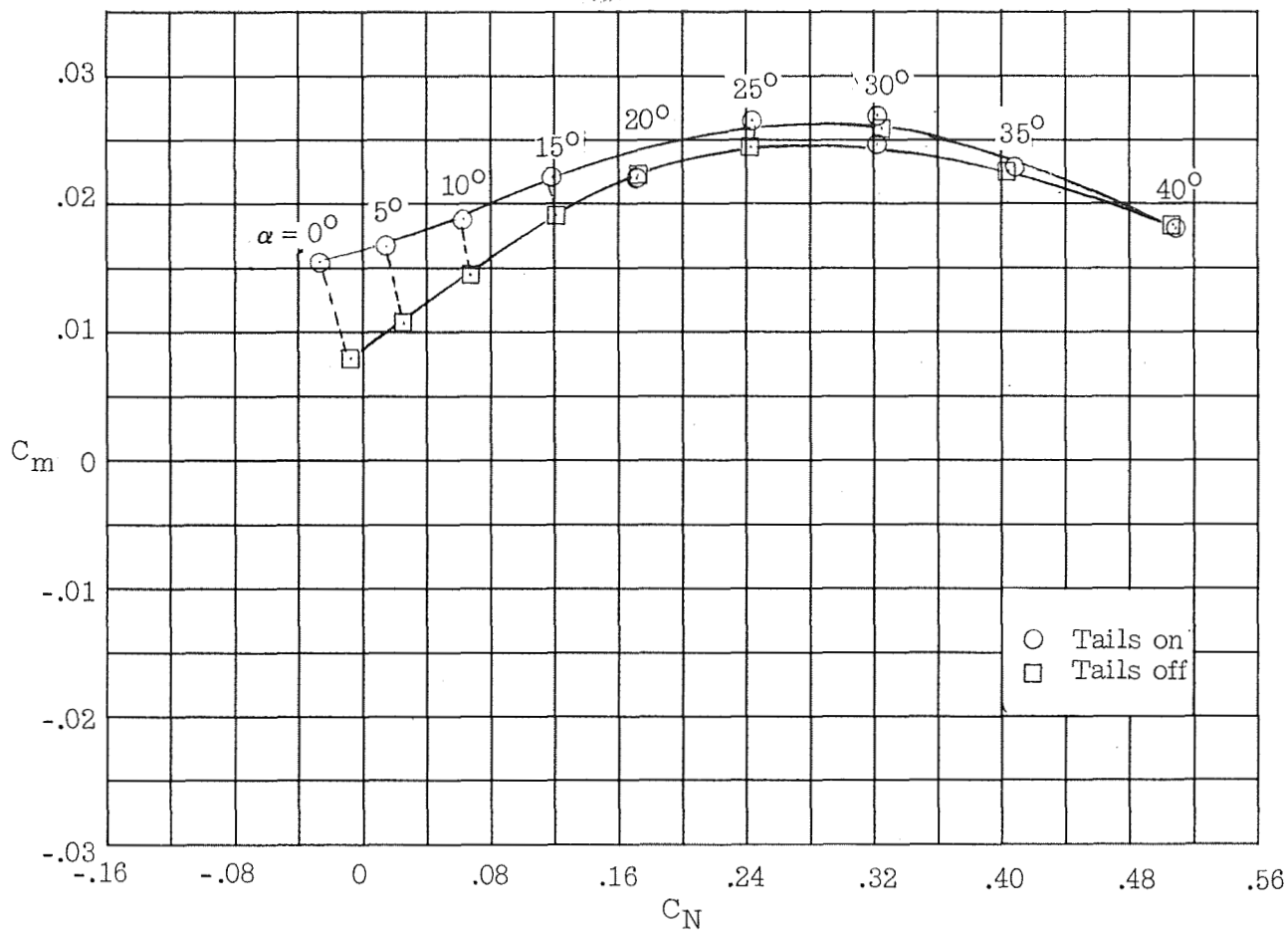
(d) Concluded.

Figure 5.- Continued.
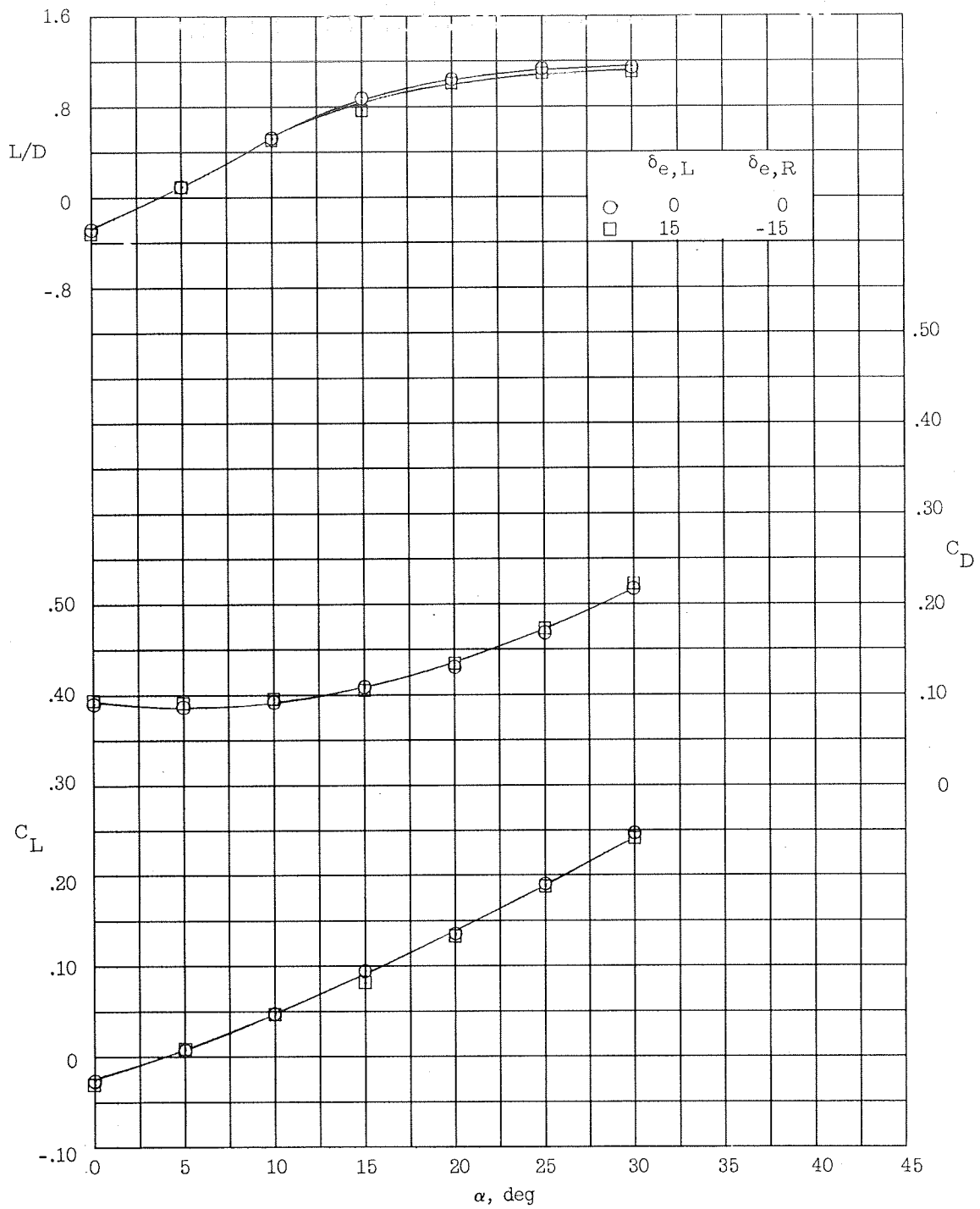
(e) Elevon-deflection effects (roll control).

Figure 5.- Continued.
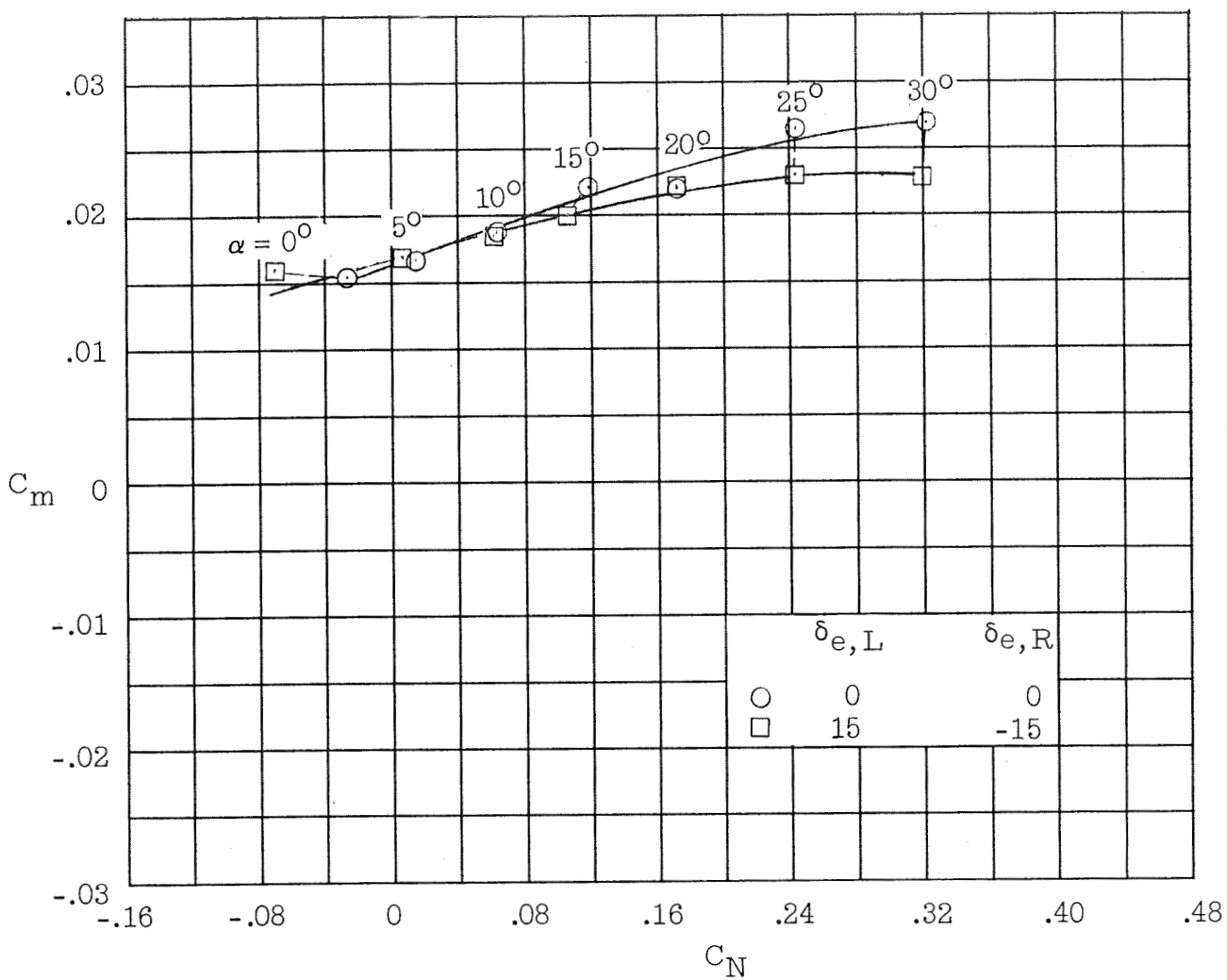
(e) Concluded.

Figure 5.- Concluded.
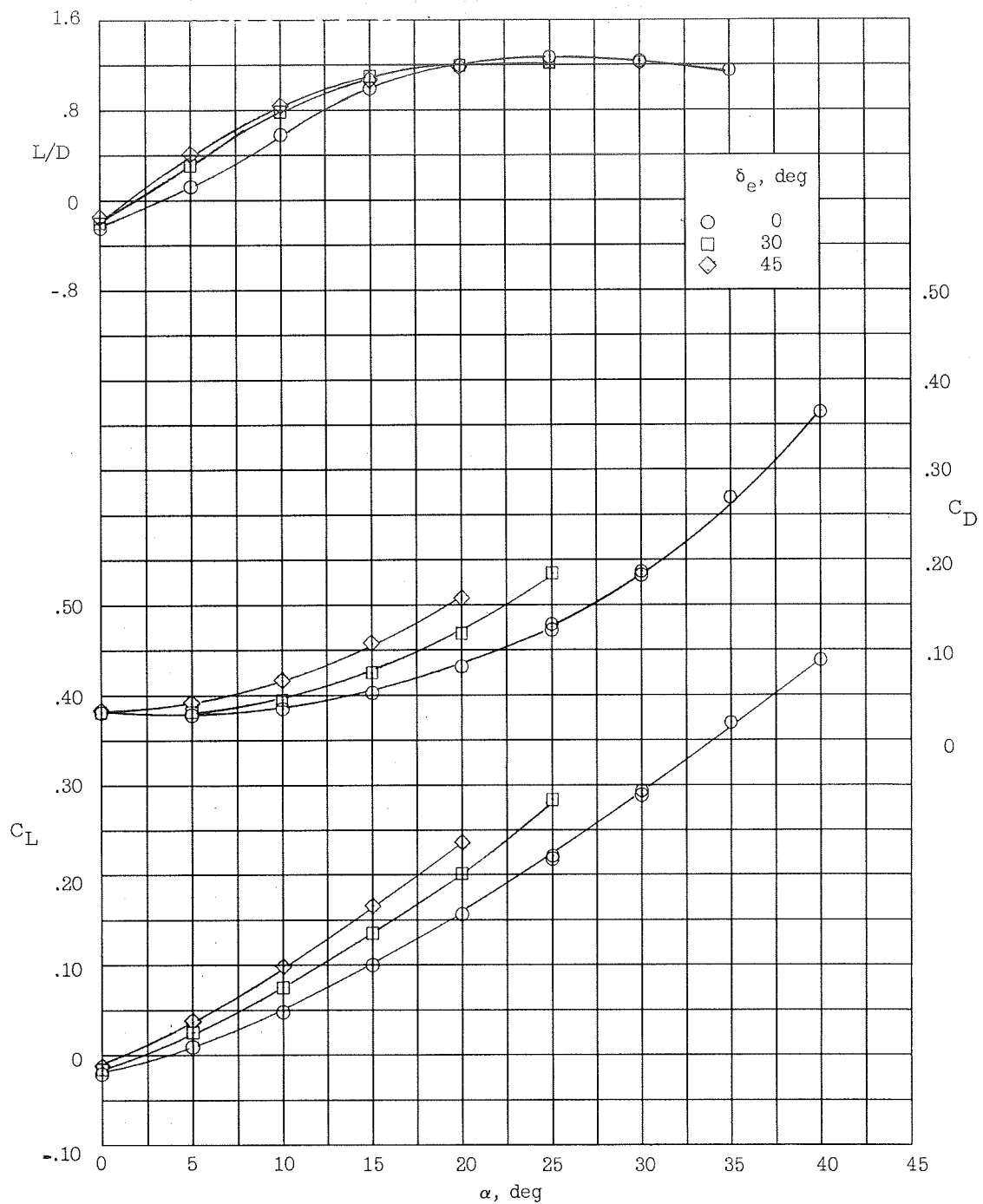
(a) Elevon-deflection effects; $\frac{S_e}{S} = 0.11$.

Figure 6.- HL-11 longitudinal aerodynamic characteristics.
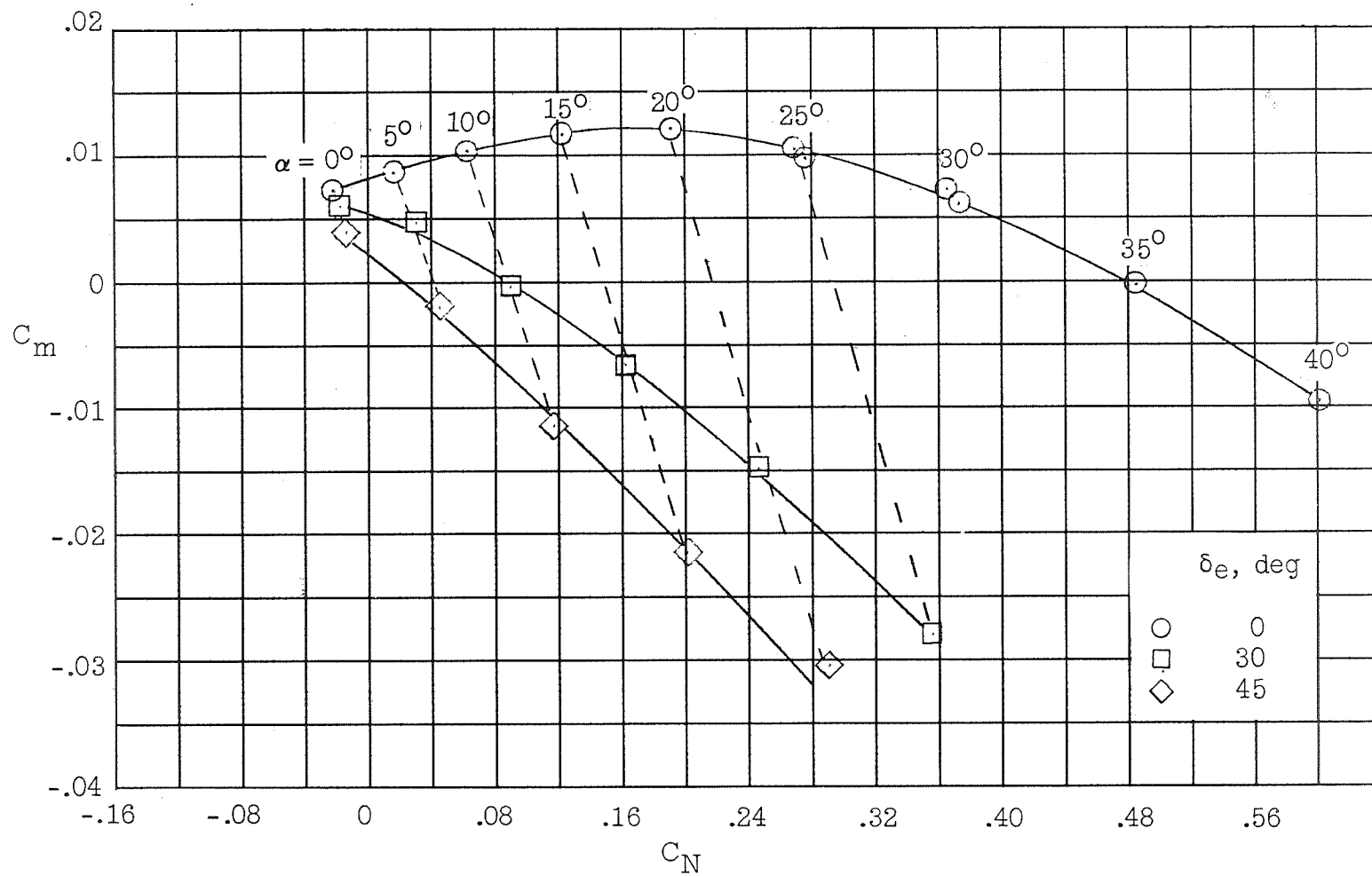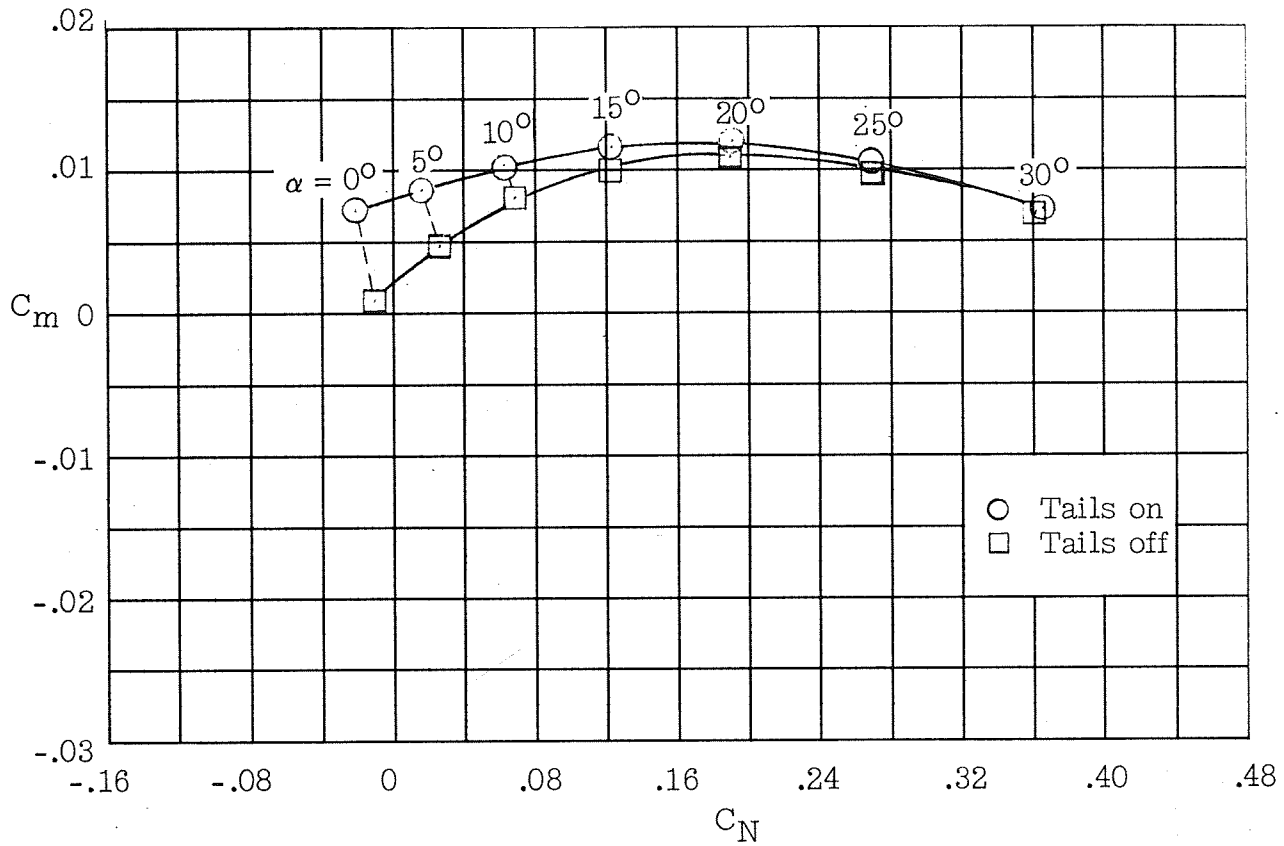
(a) Concluded.

Figure 6.- Continued.

(b) Twin-dorsal-tail effects; $\delta_e = 0^o$.
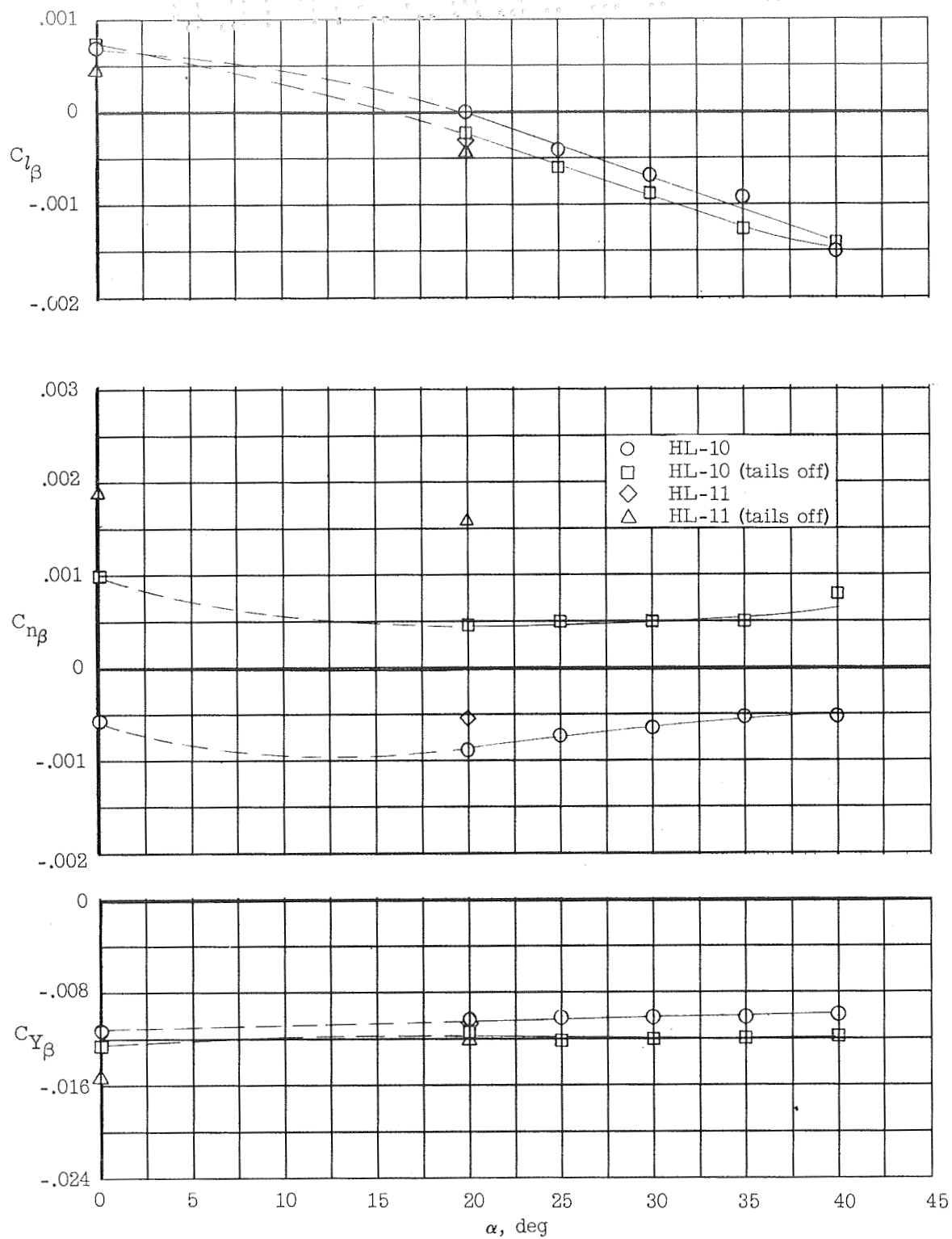
Figure 6.- Continued.

(b) Concluded.

Figure 6.- Concluded.

Figure 7.- Directional and lateral stability characteristics.
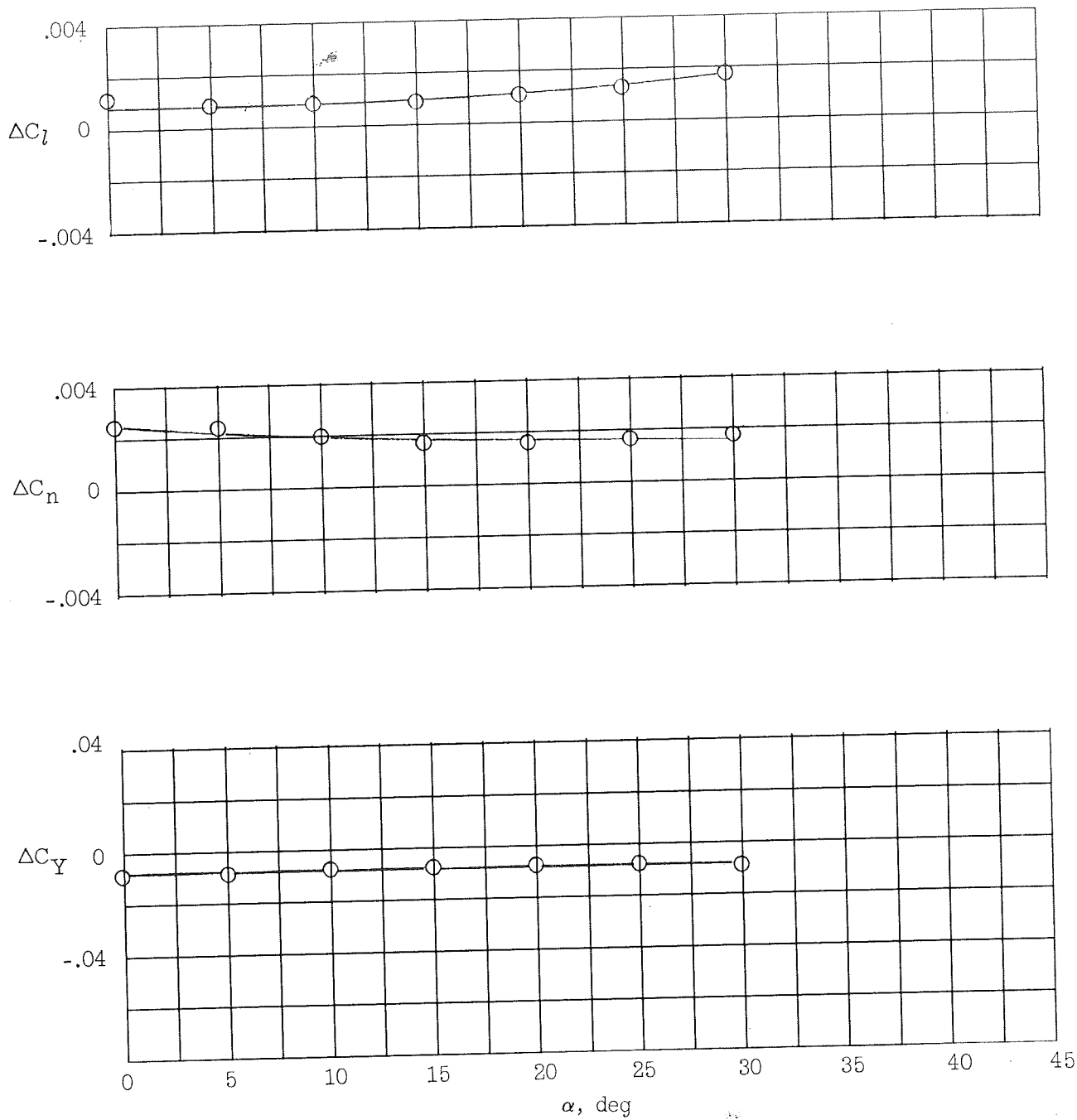
Figure 8.- Roll-control inputs for HL-10; $\frac{S_e}{S} = 0.08$.